PAPER • **OPEN ACCESS**

Simulation of mixed-mode fracture (I-II) on PFRC specimens with various fibre proportions using an embedded cohesive crack model

To cite this article: F Suárez *et al* 2019 *IOP Conf. Ser.: Mater. Sci. Eng.* **596** 012007

IOP Conf. Series: Materials Science and Engineering **596** (2019) 012007 doi:10.1088/1757-899X/596/1/012007

Simulation of mixed-mode fracture (I-II) on PFRC specimens with various fibre proportions using an embedded cohesive crack model

F Suárez[1] , JC Gálvez[2] , A Enfedaque[2] and MG Alberti[2]

[1]Departamento de Ingeniería Mecánica y Minera. Universidad de Jaén. Campus Científico-Tecnológico de Linares. Avda. de la Universidad (Cinturón Sur) – Linares, Spain
[2]Departamento de Ingeniería Civil-Construcción. Universidad Politécnica de Madrid. E.T.S.I. Caminos, Canales y Puertos, C/ Profesor Aranguren s/n - Madrid, Spain

E-mail: fsuarez@ujaen.es, jaime.galvez@upm.es, alejandro.enfedaque@upm.es, marcos.garcia@upm.es

Abstract. The study of fibre-reinforced concrete (FRC) has become of increasing interest in the last decades. Although it is not a new technology, it has experienced a remarkable progress with the appearance of some recommendations in the standards. More specifically, the use of polyolefin fibres has proved to increase the tensile strength of concrete without the problems usually found with steel fibres, especially those related to corrosion. This type of fibres have been studied in depth and its fracture behaviour has been successfully simulated in the past by means of an embedded crack model using a trilinear softening function. Nevertheless, these simulations have been always focused on cases where fracture took place under pure mode I conditions, namely using the classical three-point bending test on notched specimens. In this study, such embedded crack model is used to reproduce the fracture behaviour on notched specimens subjected to a modified three-point bending test that induces fracture under a combination of modes I and II. Three PFRC mixes are analysed, all of them with the same proportions of concrete components but different proportions of polyolefin fibres. The experimental and numerical diagrams properly agree and allow identifying how the increasing proportion of fibres can be reflected in the trilinear softening function that numerically drives the damage evolution.

1. Introduction

Fibre reinforced concrete is not a new idea. It has been used in practice for decades, especially with steel fibres. Nevertheless, many researchers have lately focused their interest in this technology, partially boosted by the appearance of recommendations in the late standards, such as the Spanish Code for concrete structures [1] and the Model Code [2]. These recommendations help to design fibre-reinforced concrete (FRC) structures and are encouraging engineers to consider it as an alternative to traditional reinforced concrete with steel rebars. They are especially focused on steel-fiber-reinforced concrete, but in the last years some interesting alternative materials have been proposed with success. More specifically, polyolefin fibres have proved to perform remarkably well from the mechanical point of view, overcoming some important drawbacks of the steel fibres, especially related to corrosion [3–6], which not only may reduce the durability of the structure, but also affect its aesthetical aspect, that can be of paramount importance in some cases.

The fracture behaviour of polyolefin fibre reinforced concrete (PFRC) specimens has been numerically reproduced in the past with success by using a well known embedded crack model based on the cohesive crack approach [7,8]. In those simulations, the cohesive model was defined by using a trilinear softening function that allowed reproducing the load recovery due to the fibre contribution after the concrete matrix failure and the final load decay that takes place when fibre is pulled out from concrete. These numerical studies, however, only used the classical three-point bending test for comparison, which develops fracture under pure mode-I conditions. Although recent research studies have analysed the performance of PFRC specimens under mode II conditions [9], the combination of modes I and II, that is a common situation in many real fracture problems, is not well understood and is still under study [10].

This contribution analyses the use of an embedded crack element formulation based on the cohesive zone approach for modelling fracture in PFRC specimens under fracture initiated under a combination of modes I and II. To do this, a modified version of the classical three point bending test described by the RILEM [11], more especifically type 1 tests proposed by Gálvez et al. in [12], is used on PFRC specimens. Three sets of specimens were tested, all of them with the same concrete proportioning but different fibre dosages: 3, 6 and 10 kg/m^3 . These tests were numerically reproduced by using the above-mentioned embedded crack formulation, showing good agreement with the experimental results.

2. Experimental results

In this section the experimental tests are briefly described and then the specimens and the three PFRC mixes analysed in this study presented.

2.1. The modified three-point bending test

The classical three-point bending test on notched specimens can be performed following the recommendations by the RILEM [11], which induces fracture under pure mode I conditions. This test describes a three point bending test where supports and the loading point are symmetrically disposed with respect to the notched specimen. A variation of this test was proposed in [12] to induce fracture under a combination of modes I and II. In that work, the authors proposed two variations of the model, with one of them (type 1) being a true three point bending test and with the other one (type 2) being in practice a four point bending test, since an additional support was added to modify the crack path and, thus, the interaction of modes I and II. In this study type 1 test is considered. The boundary conditions and the geometrical definition of the experimental setup can be seen in Figure 1. Figure 2 shows two specimens, before and after the test is finished.

2.2. Specimens

Three sets of specimens were tested, each of them with different proportions of polyolefin fibres: 3, 6 and 10 kg/m^3. In all cases the concrete proportioning was the same, with the fibre dosage being the only variation. Table 1 shows the composition of each set of specimens.

All specimens were prismatic of dimensions 600 mm × 150 mm × 150 mm and the fibre length was 60 mm.

Table 1. Mix proportioning.

	Cement (kg/m^3)	Limestone powder (kg/m^3)	Water (kg/m^3)	Sand (kg/m^3)	Gravel (kg/m^3)	Grit (kg/m^3)	Superplasticizer (% cem. weight)	Polyolefin fibres (kg/m^3)
PFRC-3	375	100	187.5	916	300	450	1.25	3
PFRC-6	375	100	187.5	916	300	450	1.25	6
PFRC-10	375	100	187.5	916	300	450	1.25	10

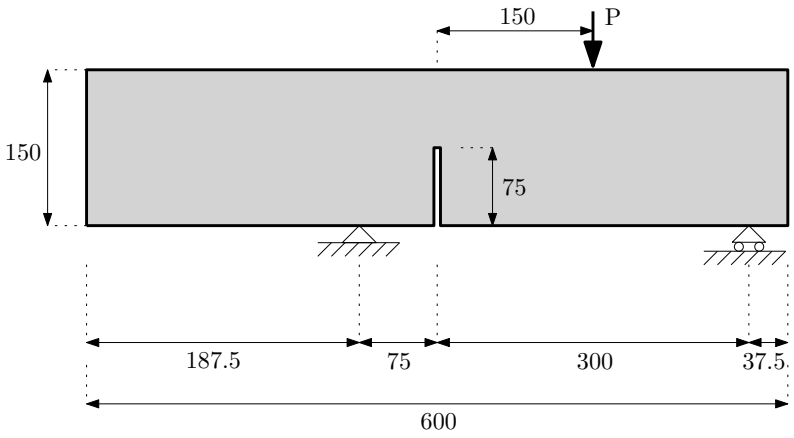

Figure 1. Set-up of the type 1 three point bending test described in [12] (dimensions in mm).

a)

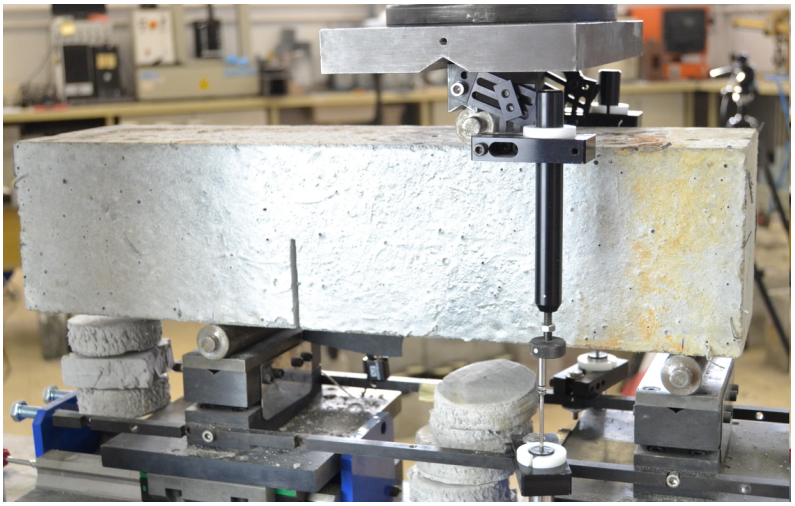

b)

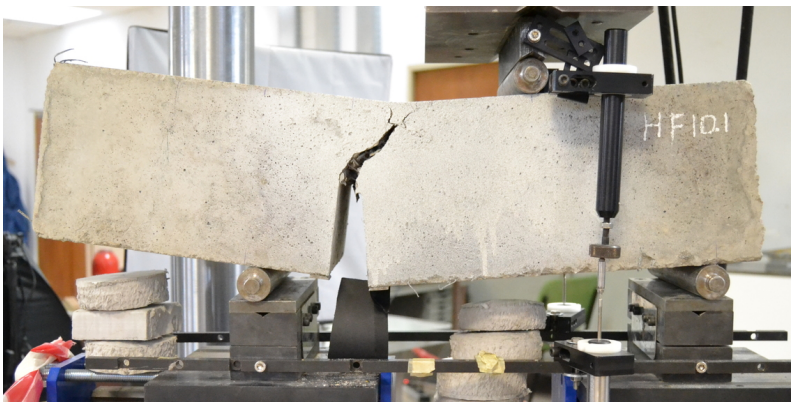

Figure 2. a) One of the tested specimens before testing, b) A specimen at the end of the test.

3. Numerical simulation

In this section the numerical work is presented. In the first place, the embedded crack formulation used to simulate cracking is briefly described and, in the second place, the finite element models are presented.

3.1. Embedded crack formulation based on the cohesive zone approach

Fracture is numerically reproduced by means of an element formulation that simulates the initiation and development of an embedded crack. This formulation is based on the cohesive zone approach and its detailed description can be consulted in [13]. In the past, the original formulation, initially designed for concrete, has been adapted to other cases, such as brickwork masonry elements [14]. Lately, it has been successfully used to simulate fibre-reinforced concrete mixes under mode I conditions [8].

This formulation is based on the cohesive zone approach proposed by Hillerborg [15] (for more information on this topic, refer to [16]). In this case, it is a central forces model, that is to say, it assumes that the cohesive stress vector $\boldsymbol{t}$ is perpendicular to the crack opening and parallel to the crack displacement vector $\boldsymbol{w}$:

$$\boldsymbol{t} = \frac{f(\tilde{w})}{\tilde{w}}\boldsymbol{w} \qquad \text{with } \tilde{w} = \max(|\boldsymbol{w}|) \tag{1}$$

with $f(|\tilde{w}|)$ representing the material softening function, which is expressed in terms of an equivalent crack opening $\tilde{w}$ that stores the maximum historical crack opening and allows accounting for possible unloading processes. When simulating PFRC specimens, this softening function presents three linear branches [7] as shown in Figure 3, and can be expressed by:

$$\sigma = \begin{cases} f_{ct} + \left(\dfrac{\sigma_k - f_{ct}}{w_k}\right) \cdot w & \text{if } 0 < w \leq w_k \\ \sigma_k + \left(\dfrac{\sigma_r - \sigma_k}{w_r - w_k}\right) \cdot (w - w_k) & \text{if } w_k < w \leq w_r \\ \sigma_r + \left(\dfrac{-\sigma_r}{w_f - w_r}\right) \cdot (w - w_r) & \text{if } w_r < w \leq w_f \\ 0 & \text{if } w > w_f \end{cases} \tag{2}$$

In the models that are presented later, constant strain triangular elements are used; in this case crack can only develop in directions parallel to one of the triangle sides and at mid height, which guarantees local and global equilibria and reduces to three the possible crack paths in an element (see Figure 4).

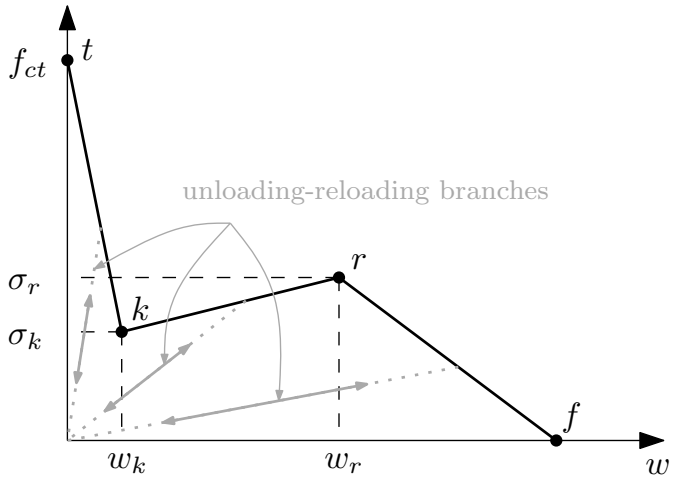

Figure 3. Trilinear softening function.

Once the cracking process starts, the element is divided into two parts, A^+ and A^-. If A stands for the element area, h for the height of the triangle perpendicular to the opposite side to the solitary node, L for the crack length and $\boldsymbol{n}$ for the unit vector perpendicular to the crack, vector $\boldsymbol{t}$ is constant along the crack and can be obtained as:

$$\boldsymbol{t} = \frac{A}{hL}\boldsymbol{\sigma}\cdot\boldsymbol{n} \tag{3}$$

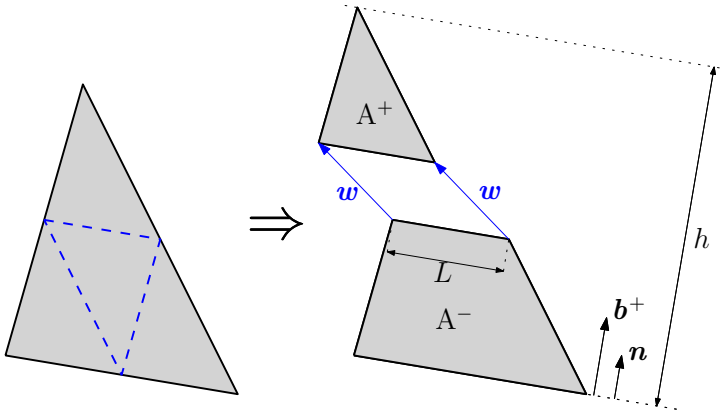

Figure 4. Potential crack paths (left) and geometrical definitions of $\boldsymbol{w}$, $\boldsymbol{n}$ and $\boldsymbol{b}^+$ (right).

The part of the element outside the crack behaves as linear-elastic and the crack displacement vector $\boldsymbol{w}$ can be obtained subtracting the contribution of the crack to the elastic prediction of the stress:

$$\boldsymbol{\sigma} = \boldsymbol{E} : \left[\epsilon^a - \left(\boldsymbol{b}^+ \otimes \boldsymbol{w}\right)^S\right] \tag{4}$$

where $\boldsymbol{E}$ stands for the elastic tangent tensor, $\boldsymbol{b}^+$ for the gradient vector of the solitary node shape function, expressed by (5), ϵ^a for the apparent strain vector. In this expression superscript S indicates the symmetric part of the tensor, : the usual double-dot product ($(\boldsymbol{A}:\boldsymbol{b})_{ij} = A_{ijkl}b_{kl}$) and $\otimes$ the usual direct product ($(\boldsymbol{a}\otimes\boldsymbol{b})_{ij} = a_i b_j$).

$$\boldsymbol{b}^{+} = \frac{1}{h}\boldsymbol{n} \tag{5}$$

In addition, $\boldsymbol{t}$ can be obtained as $\boldsymbol{t} = \boldsymbol{\sigma} \cdot \boldsymbol{n}$, by using (1) and (4):

$$\frac{f(\tilde{w})}{\tilde{w}}\boldsymbol{w} = [\boldsymbol{E} : \boldsymbol{\epsilon}^{a}] \cdot \boldsymbol{n} - \left[\boldsymbol{E} : \left(\boldsymbol{b}^{+} \otimes \boldsymbol{w}\right)^{S}\right] \cdot \boldsymbol{n}$$

which can be rewritten as:

$$\left[\frac{f(\tilde{w})}{\tilde{w}}\mathbf{1} + \boldsymbol{n} \cdot \boldsymbol{E} \cdot \boldsymbol{b}^{+}\right] \cdot \boldsymbol{w} = [\boldsymbol{E} : \boldsymbol{\epsilon}^{a}] \cdot \boldsymbol{n} \tag{6}$$

with $\mathbf{1}$ being the second-order identity tensor.

3.2. FEM models

The embedded crack formulation described above was implemented by means of a UMAT subroutine to be used in Abaqus® and the specimens were simulated with bi-dimensional models using reduced integration triangular elements. In these models, all elements are of the same material, which follows the formulation presented above and are characterised by the same material parameters.

To compare the experimental and the numerical results, the evolution of load with respect to two displacement measurements are analysed: the crack mouth opening displacement (CMOD) and the vertical displacement of the loading point. From the experimental point of view, the CMOD is measured by means of a strain gauge and the loading point displacement by means of a linear variable differential transducer (LVDT). It must be noted that the CMOD is not only a horizontal displacement in this case (it is in the classical symmetrical disposition described in [11], but not in the present case); this must be taken into account when obtaining the diagrams from the numerical results. Figure 5 shows one of the meshes used and the position of the supports and the loading point.

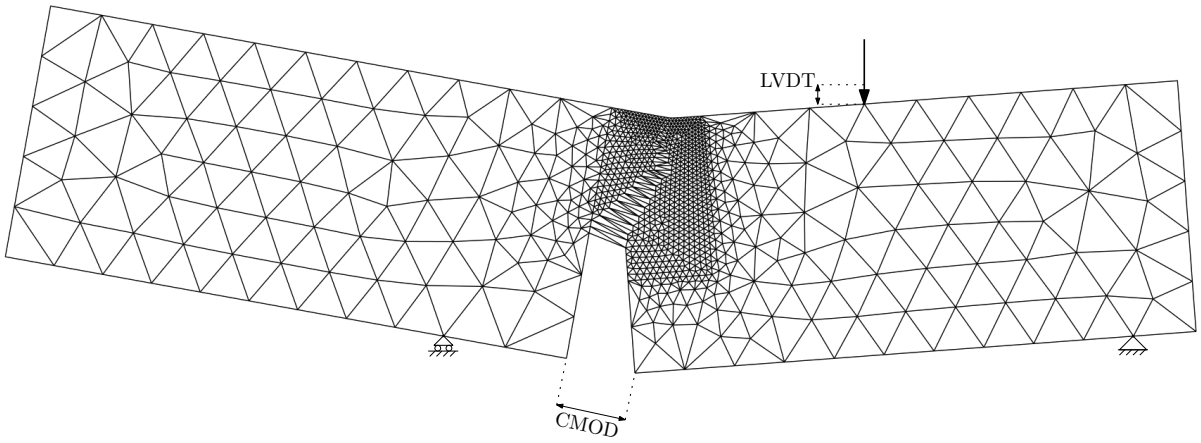

Figure 5. Deformed mesh of one of the models used in this study. The loading and boundary conditions are displayed, as well as the LVDT and CMOD measurements.

The softening function has been defined as trilinear and their characteristic points can be consulted in Table 2 and observed in Figure 6. To calibrate these points the following criteria has been followed: initial and final points, t and f , are equal in all three diagrams, only points k and r are different in order to account for different fibre proportions.

Table 2. Characteristic points of the trilinear softening functions used with each fibre dosage.

	PFRC-3				PFRC-6				PFRC-10			
	t	k	r	f	t	k	r	f	t	k	r	f
w (mm)	0.00	0.15	2.250	7.50	0.00	0.14	2.250	7.50	0.00	0.13	2.250	7.50
σ (MPa)	2.30	0.12	0.245	0.00	2.30	0.33	0.700	0.00	2.30	0.75	1.700	0.00

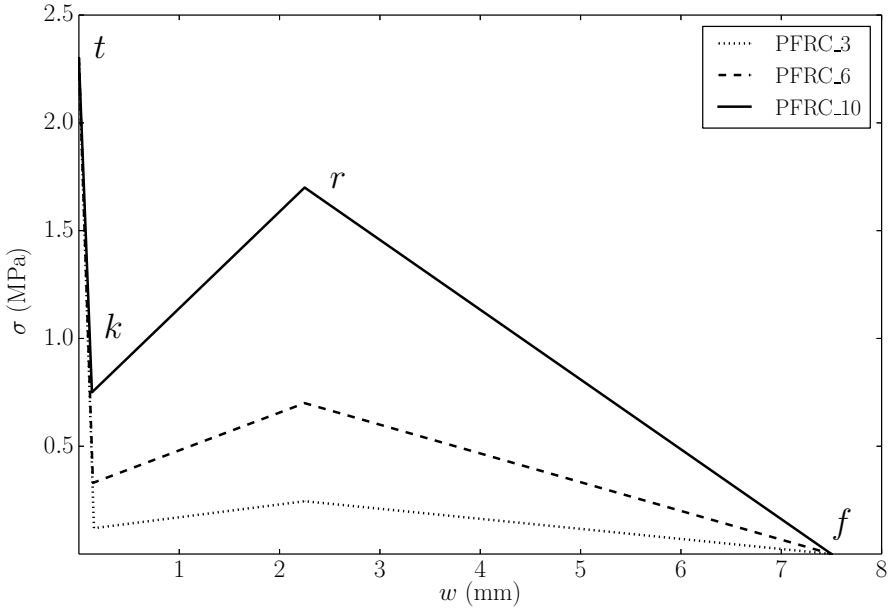

Figure 6. Trilinear softening diagrams used to simulate each fibre proportion.

4. Results

Figures 7 and 8 compare the load-CMOD and load-LVDT diagrams obtained experimentally and numerically. These figures show that the softening functions of Figure 6 provide an adequate approximation to the experimental behaviour of the three analysed concrete mixes. The peak load is properly reproduced in all cases, as well as the load decrease after the concrete matrix initial failure. Regarding the later behaviour, all numerical simulations remain inside the experimental envelope, no matter if the CMOD or the LVDT displacement is used for comparison. The numerical results reproduce adequately the load increase due to the performance of the polyolefin fibres as well as the later load decay that takes place as a result of the pulling out of the fibres.

Finally, Figure 9 shows the crack path obtained numerically (damaged elements are shaded in blue) and the experimental envelope of the crack paths (overlapped in red) for each PFRC mix. The initial branches of these paths obtained numerically are in all cases reasonably accurate when compared with the experimental envelopes, although the path deviates considerably for later stages of the tests. It must be born in mind that in PFRC specimens the fracture path is highly influenced by the local presence of fibres around the crack tip during the test, which can explain these differences.

5. Final remarks

The results presented in this contribution confirm the validity of trilinear softening functions with PFRC specimens subjected to a modified three-point bending test that induces fracture

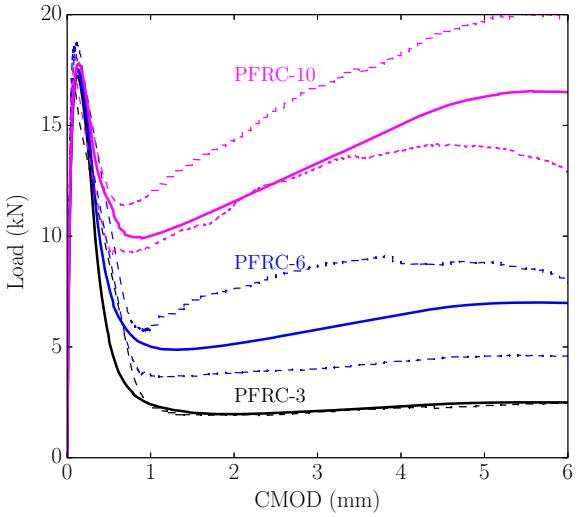

Figure 7. Comparison of Load-CMOD diagrams obtained experimentally and numerically for each fibre dosage.

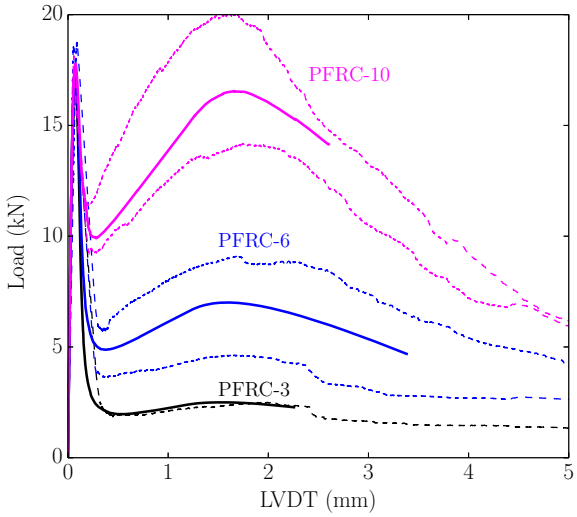

Figure 8. Comparison of Load-LVDT diagrams obtained experimentally and numerically for each fibre dosage.

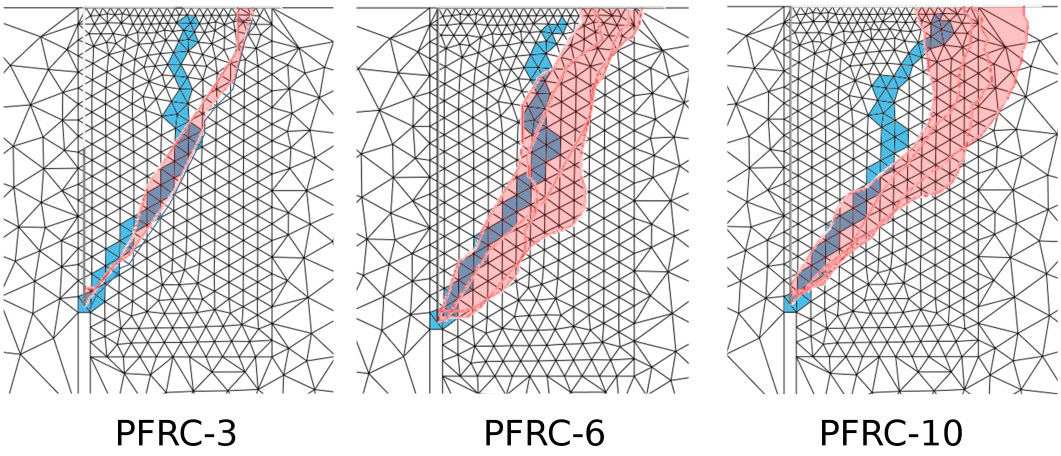

Figure 9. Comparison of the crack paths obtained experimentally and numerically for each of the analysed PFRC mixes.

under mixed-mode (I+II) conditions. This observation has been confirmed with PFRC mixes of the same concrete proportioning but various fibre dosages: 3, 6 and 10 kg/m^3 . Only modifying the two intermediate points of the softening function is enough to adjust the fibre behaviour of each fibre proportion.

Acknowledgements

The authors gratefully acknowledge the financial contribution for this Research provided by the Ministry of Economy and Competitiveness of Spain by means of the Research Fund Project BIA2016-78742-C2-2-R. They also thank SIKA SAU for supplying the polyolefin fibres used in the experimental work.

References

[1] EHE-08. Instrucción de hormigón estructural. *Ministerio de Fomento, Madrid, España*, 2008.
[2] Paul Beverly. *fib model code for concrete structures 2010*. Ernst & Sohn, 2013.
[3] M.G. Alberti, A. Enfedaque, and J.C. Gálvez. On the mechanical properties and fracture behavior of polyolefin fiber-reinforced self-compacting concrete. *Construction and Building Materials*, 55:274 – 288, 2014.
[4] M.G. Alberti, A. Enfedaque, and J.C. Gálvez. Comparison between polyolefin fibre reinforced vibrated conventional concrete and self-compacting concrete. *Construction and Building Materials*, 85:182 – 194, 2015.
[5] A. Enfedaque, M.G. Alberti, J.A. Paredes, and J.C. Gálvez. Interface properties of polyolefin fibres embedded in self-compacting concrete with a bond improver admixture. *Theoretical and Applied Fracture Mechanics*, 90:287 – 293, 2017.
[6] A. Enfedaque, M.G. Alberti, J. Gálvez, M. Rivera, and J. Simón-Talero. Can polyolefin fibre reinforced concrete improve the sustainability of a flyover bridge? *Sustainability*, 10(12):4583, 2018.
[7] M.G. Alberti, A. Enfedaque, J.C. Gálvez, and E. Reyes. Numerical modelling of the fracture of polyolefin fibre reinforced concrete by using a cohesive fracture approach. *Composites Part B: Engineering*, 111:200– 210, 2017.
[8] A. Enfedaque, M.G. Alberti, J.C. Gálvez, and J. Domingo. Numerical simulation of the fracture behaviour of glass fibre reinforced cement. *Construction and Building Materials*, 136:108 – 117, 2017.
[9] A. Picazo, J.C. Gálvez, M.G. Alberti, and A. Enfedaque. Assessment of the shear behaviour of polyolefin fibre reinforced concrete and verification by means of digital image correlation. *Construction and Building Materials*, 181:565 – 578, 2018.
[10] F. Suárez, J.C. Gálvez, A. Enfedaque, and M.G. Alberti. Modelling fracture on polyolefin fibre reinforced concrete specimens subjected to mixed-mode loading. *Engineering Fracture Mechanics*, 211:244 – 253, 2019.
[11] RILEM. Determination of the fracture energy of mortar and concrete by means of three-point bend tests on notched beams. *Mater Struct*, 18(106):285–290, 1985.
[12] J.C. Gálvez, M. Elices, G. Guinea, and J. Planas. Mixed mode fracture of concrete under proportional and nonproportional loading. *Int J Fract*, 94(3):267–284, 1998.
[13] J.M. Sancho, J. Planas, D.A. Cendón, E. Reyes, and J.C. Gálvez. An embedded crack model for finite element analysis of concrete fracture. *Engineering Fracture Mechanics*, 74(1):75 – 86, 2007. Fracture of Concrete Materials and Structures.
[14] E. Reyes, J.C. Gálvez, M.J. Casati, D.A. Cendón, J.M. Sancho, and J. Planas. An embedded cohesive crack model for finite element analysis of brickwork masonry fracture. *Engineering Fracture Mechanics*, 76(12):1930 – 1944, 2009.
[15] A. Hillerborg, M. Modéer, and P.-E. Petersson. Analysis of crack formation and crack growth in concrete by means of fracture mechanics and finite elements. *Cem Concr Res*, 6(6):773 – 781, 1976.
[16] Zdeněk P Bažant and Jaime Planas. *Fracture and size effect in concrete and other quasibrittle materials*. CRC Press, 1997.